



AIAA 2000-0504

**Development of a Flush Airdata Sensing
System on a Sharp-Nosed Vehicle for
Flight at Mach 3 to 8**

Mark C. Davis, Joseph W. Pahle,
John Terry White, and Laurie A. Marshall
NASA Dryden Flight Research Center
Edwards, California

Michael J. Mashburn
Micro Craft, Inc.
Tullahoma, Tennessee

Rick Franks
Sverdrup Corp.
Arnold Air Force Base, Tennessee

**38th Aerospace Sciences
Meeting and Exhibit**
10–13 January 2000 / Reno, NV

DEVELOPMENT OF A FLUSH AIRDATA SENSING SYSTEM ON A SHARP-NOSED VEHICLE FOR FLIGHT AT MACH 3 TO 8

Mark C. Davis,* Joseph W. Pahle,[†] John Terry White,[‡] and Laurie A. Marshall[§]

NASA Dryden Flight Research Center
Edwards, California

Michael J. Mashburn[¶]

Micro Craft, Inc.
Tullahoma, Tennessee

Rick Franks[#]

Sverdrup Corp.
Arnold Air Force Base, Tennessee

Abstract

NASA Dryden Flight Research Center has developed a flush airdata sensing (FADS) system on a sharp-nosed, wedge-shaped vehicle. This paper details the design and calibration of a real-time angle-of-attack estimation scheme developed to meet the onboard airdata measurement requirements for a research vehicle equipped with a supersonic-combustion ramjet engine. The FADS system has been designed to perform in flights at Mach 3–8 and at -6° – 12° angle of attack. The description of the FADS architecture includes port layout, pneumatic design, and hardware integration. Predictive models of static and dynamic performance are compared with wind-tunnel results across the Mach and angle-of-attack range. Results indicate that static angle-of-attack accuracy and pneumatic lag can be adequately characterized and incorporated into a real-time algorithm.

*Aerospace Engineer.

[†]Aerospace Engineer, Senior Member.

[‡]Engineering Consultant, Senior Member.

[§]Aerospace Engineer.

[¶]Instrumentation and Controls Engineer.

[#]Instrumentation Engineer.

Copyright © 2000 by the American Institute of Aeronautics and Astronautics, Inc. No copyright is asserted in the United States under Title 17, U.S. Code. The U.S. Government has a royalty-free license to exercise all rights under the copyright claimed herein for Governmental purposes. All other rights are reserved by the copyright owner.

Nomenclature

Acronyms

FADS	flush airdata sensing
INS	inertial navigation system
PPT	precision pressure transducer
SCRamjet	supersonic-combustion ramjet

Symbols

C_{PPT}	transducer calibration as a function of Mach number
D	diameter of lines from port to transducer, in.
$FADS_{\alpha_1}$	angle of attack at front of vehicle, deg
$FADS_{\alpha_2}$	angle of attack at rear of vehicle, deg
$FADS_{\alpha_3}$	angle of attack for pseudodifferential transducers, deg
g	acceleration caused by gravity, ft/sec^2
i	arbitrary integer
k	lag constant
L	pneumatic line
L	length, ft
P_{PPT}	measured pressure at transducer, lbf/ft^2
P_{port}	measured pressure at port, lbf/ft^2
\bar{q}	dynamic pressure, lbf/ft^2

q_1	weighting function
s	Laplace frequency variable
V_e	effective volume of the measurement system, ft ³
X/L	body axis location
α	angle of attack, deg
α_{est}	bias angle of attack, deg
α_{FADS}	reference angle of attack derived from the FADS algorithm, deg
α_{INS}	angle of attack derived from the inertial navigation system, deg
α_{true}	angle of attack obtained from wind tunnel, deg
α_1	forward angle-of-attack estimate, deg
α_2	rear angle-of-attack estimate, deg
α_3	pseudodifferential angle-of-attack estimate, deg
β	angle of sideslip, deg
Δ	difference
μ	dynamic viscosity of the air in the line, lbm/(ft/sec)
τ	time constant

Introduction

The National Aeronautics and Space Administration and aerospace community are developing air-breathing propulsion systems capable of flight at hypersonic speeds. One promising concept is the supersonic-combustion ramjet (SCRamjet) engine.¹ The current design of SCRamjets allows supersonic combustion to occur only in a narrow operating range.

Dynamic pressure (\bar{q}) and angle of attack (α) are two of the critical parameters that determine the flow into the engine inlet. Accurate measurement of these parameters is desired for real-time control and is required for postflight analysis. Accurately estimating angle of attack from the inertial navigation system (INS) alone is difficult because of atmospheric variations and sensor installation and performance.² This requirement led to the development of a nonintrusive system, the flush airdata sensing (FADS) system, that has the ability to measure angle of attack in real time and allow the remainder of the airdata parameters to be reconstructed postflight.

The FADS concept uses a matrix of flush surface ports to infer airdata. The FADS system has been successfully applied to a variety of blunt forebodies,^{3–7} and one feasibility study¹ has been conducted for a sharp-nosed, hypersonic configuration. To be a viable system, the FADS system must measure angle of attack to within 0.5° (because of the criticality of incidence angle of the engine inlet); measure dynamic pressure to within 5 percent for postflight analysis; and survive the intense thermal environment in which a hypersonic vehicle flies.⁸ This paper presents the architecture, estimation algorithms, and wind-tunnel calibration of a FADS system intended for a sharp-nosed, SCRamjet test vehicle.

Note that use of trade names or names of manufacturers in this document does not constitute an official endorsement of such products or manufacturers, either expressed or implied, by the National Aeronautics and Space Administration.

Flush Airdata Sensing System Architecture Overview

This section describes the pneumatic architecture of the FADS system. The port layout, the sensing transducer characteristics, and the pneumatic layout of the pressure sensing system are described. The sensing components that comprise the real-time airdata system are distinguished from those used for the postflight algorithm.

Pressure Port Layout

A matrix of nine pressure ports is used to sense the airdata parameters. Figure 1 shows the locations of these ports on the vehicle forebody. Four ports (indicated by the highlighted symbols along the centerline of the forebody in figure 1) are used to indirectly sense the angle of attack. The remaining five pressure ports (indicated by the open symbols in figure 1) are used for postflight evaluation of the remaining airdata parameters. To save real-time bandwidth and ensure a high data throughput, the system architecture decouples the angle-of-attack estimation from the remainder of the postflight algorithm. Only the pressure data from the angle-of-attack ports is used in real time and combined with the inertial angle of attack to estimate a high-fidelity, vehicle angle of attack.

Pressure Transducers

The nine pressures are sensed using a combination of absolute and differential precision pressure transducers

(PPTs). Figure 2 shows the pneumatic layout of these sensors. Differences between the pairs of upper and lower ramp surface pressures (ports 2 and 4; ports 3 and 5) are sensed by differential pressure transducers to provide high accuracy and a high-resolution measurement for use by the real-time algorithm. Each differential pair is also “teed” to an absolute pressure transducer that allows the absolute pressure level at each port to be sensed or calculated. The forebody side ports (ports 6 and 8; ports 7 and 9), although not used by the real-time algorithm, are sensed in a similar manner. The single stagnation pressure (port 1) is sensed using an absolute sensor.

All of the pressure transducers have serial digital outputs, which are connected through an individually addressable, multidrop RS-485 bus. The sensors also provide an optional analog output. The PPT digital output is the primary signal used in the real-time and postflight algorithms. The analog signal is recorded only for postflight analysis and provides data redundancy if the digital signal fails. The pressure transducers use a piezo-resistive bridge technology and have a built-in digital temperature compensation over a range from -40 to 80 °C.

The manufacturer’s specified accuracy for the sensor output for both digital and analog is 0.05 percent of full scale.⁹ Laboratory tests conducted at the NASA Dryden Flight Research Center (Edwards, California) have shown the sensors to be accurate to within 0.025 percent of the full-scale value. Table 1 shows the types of sensors used in this design and the sensor full-scale

Table 1. Sensor type at each port location.

Sensor identification	Port	Parameter sensed	Sensor type	Range, lbf/in ²
PPT 1	1	Total pressure	Absolute	0–15
PPT 2 *	2, 4	α	Differential	± 5
PPT 3 *	2	α	Absolute	0–15
PPT 4 *	3, 5	α	Differential	± 5
PPT 5 *	5	α	Absolute	0–15
PPT 6	6, 8	β	Differential	± 5
PPT 7	6	β	Absolute	0–15
PPT 8	7, 9	β	Differential	± 5
PPT 9	9	β	Absolute	0–15

ranges. The sensors used as a part of the real-time system architecture are indicated with an asterisk.

Pneumatic Layout

Table 2 shows the line lengths, tubing diameters, and entrapped volumes for the various pneumatic components (fig. 2). The effective volume in table 2 also includes the entrapped volume of the pneumatic fittings and the transducer volumes. Results from preliminary oblique shock theory¹⁰ and engineering judgment were used in the placement of the pressure ports on the vehicle. The pressure port size on the upper and lower ramp surfaces was 0.04-in. diameter. The pressure port size on the leading edge and sides of the vehicle had a diameter of 0.02 in. to limit stagnation heating effects. All ports were drilled normal to the surface.

The “teed” pneumatic lines required to obtain the absolute pressure levels for ports 3 and 5 and 6 and 8 are a cause for concern because of latencies that may be introduced into the sensed pressure signals. These latencies are especially critical for the real-time sensing system. The effects of these latencies will be analyzed in detail in the Results and Discussion section.

Table 2. Pneumatic layout characteristics.

Line number	Line length, in.	Tube diameter, in.	Volume, in ³
L1A	84	0.063	0.3502
L2A	45	0.063	0.2381
L2B	37	0.063	0.2049
L3A	44	0.063	0.2340
L4A	16	0.063	0.1176
L4B	25	0.063	0.1550
L5A	24	0.063	0.1509
L6A	36	0.063	0.2007
L6B	38	0.063	0.2090
L7A	37	0.063	0.2049
L8A	36	0.063	0.2007
L8B	24	0.063	0.1509
L9A	35	0.063	0.1966

Wind-Tunnel Facilities, Equipment, Test Conditions, and Procedures

This section describes the facilities, procedures, equipment, and tests conditions for a series of wind-tunnel experiments conducted to evaluate the FADS system. The basic measurement systems were evaluated over a broad range of Mach numbers, and a data set allowing a preliminary airdata calibration was obtained.

Facilities

All wind-tunnel testing occurred at the Arnold Engineering Development Center (Arnold Air Force Base, Tennessee) Von Karman Facility in tunnels A and B. Tunnel A is a 40- by 40-in., continuous, closed-circuit, variable-density, supersonic wind tunnel with a Mach number range of 1.5 to 5.5. The tunnel is served by a main compressor system that provides a wide range of mass flow and stagnation pressures to a maximum of 195 lbf/in² absolute.¹¹

Tunnel B is a continuous, closed-circuit, hypersonic wind tunnel with a 50-in.-diameter test section. Tunnel B uses two axisymmetric, contoured nozzles that provide two fixed Mach numbers of 6 and 8 with an operating pressure range of 20 to 300 lbf/in² absolute at Mach 6 and 50 to 900 lbf/in² absolute at Mach 8.¹¹

Wind-Tunnel Test Equipment

Figure 3 shows the internal layout of the test article with nine PPTs and one inclinometer. The sensors were enclosed in cooling jackets to ensure that the sensor operating limits were not exceeded during the test. An inclinometer measured the model incidence angle over a range of $\pm 14.5^\circ$ with an accuracy of 0.02-percent full scale. The model used in the test was an 80-percent-scale model of the SCRamjet test vehicle forebody. The model was designed for hypersonic testing for extended periods. The model was milled from solid bar stock of heat-treated and solution-annealed 316 stainless steel.¹² The model had a boundary-layer trip strip installed just aft of pressure port 4 (fig. 1). The wind-tunnel pneumatic system was designed to duplicate the flight hardware.

Analog and digital outputs from the PPTs were sensed during the wind-tunnel tests. Digital data were polled from all PPTs at a rate of 48.8 samples/sec. Analog data were obtained using a 16-bit analog-to-digital converter unit controlled by the wind-tunnel

computer. Figure 4 shows a schematic of the data acquisition system used for the wind-tunnel tests. Figures 5 and 6 show the model as mounted in tunnels A and B for testing.

Wind-Tunnel Test Procedures and Conditions

Wind-tunnel data were taken during constant angles of attack and sideslip and during pitch-pause runs with sweeps in angles of attack and sideslip. Data were obtained over a Mach number range of 3 to 8, an angle-of-attack range of -6° to 12° , and an angle-of-sideslip range of $\pm 3^\circ$. In the pitch-pause maneuvers, data were obtained in 1-deg increments. Angle-of-sideslip data were obtained in 0.5-deg increments. The dwell time at each pitch-pause data point was approximately 15 sec. Table 3 shows the wind-tunnel conditions.

Real-Time Angle-of-Attack Estimation Algorithm

The primary function of the real-time angle-of-attack estimation algorithm is to provide a pneumatically-based measurement estimate of the bias in the INS-derived angle of attack. The real-time FADS algorithm is composed of two basic routines, FADS calibration and signal selection. These algorithms require Mach number, which is provided by the INS. At relatively high velocities, inertial Mach number is sufficiently accurate when used with a representative atmospheric model.

For the sensor configuration shown in figure 2, only three unique angle-of-attack estimates are available, although four pressure ports and four pressure sensors are designated for real-time angle-of-attack estimation. The individual angle-of-attack measurements are as follows:

$$\begin{aligned}\alpha_1 &= \left[\frac{(P_{PPT\ 2})}{\bar{q}} \right] C_{PPT\ 2} \\ \alpha_2 &= \left[\frac{(P_{PPT\ 4})}{\bar{q}} \right] C_{PPT\ 4} \\ \alpha_3 &= \left[\frac{(P_{PPT\ 3} - P_{PPT\ 5})}{\bar{q}} \right] C_{PPT\ 53}\end{aligned}, \quad (1)$$

where α_1 is the forward angle-of-attack estimate, α_2 is the rear angle-of-attack estimate, and α_3 is the pseudodifferential angle-of-attack estimate.

Table 3. Wind-tunnel test summary.

Test condition	Mach number					Remark	Reynolds number, mil/ft
	3	4	5	6	8		
β sweep at $-6^\circ \alpha$	x	x	x	x	x	Basic	3.00
β sweep at $-4^\circ \alpha$	x	x	x	x	x	Basic	3.00
β sweep at $-2^\circ \alpha$	x	x	x	x	x	Basic	3.00
β sweep at $0^\circ \alpha$	x	x	x	x	x	Basic	3.00
β sweep at $2^\circ \alpha$	x	x	x	x	x	Basic	3.00
β sweep at $4^\circ \alpha$	x	x	x	x	x	Basic	3.00
β sweep at $6^\circ \alpha$	x	x	x	x	x	Basic	3.00
β sweep at $8^\circ \alpha$	x	x	x	x	x	Basic	3.00
β sweep at $10^\circ \alpha$	x	x	x	x	x	Basic	3.00
β sweep at $12^\circ \alpha$	x	x	x	x	x	Basic	3.00
α sweep at $0^\circ \beta$	x	x	x	x	x	Hysteresis/ Lag effects	3.00
α sweep at $3^\circ \beta$	x	x	x	x	x	Hysteresis/ Lag effects	3.00
α sweep at $0^\circ \beta$	x	x	x			Reynolds number effects	1.80
α sweep at $3^\circ \beta$	x	x	x			Reynolds number effects	1.80
α sweep at $0^\circ \beta$		x	x			Reynolds number effects	3.76
α sweep at $3^\circ \beta$		x	x			Reynolds number effects	3.76

Figure 7 shows the angle-of-attack estimation algorithm in block diagram form. For PPT 2, PPT 4, and the difference between PPT 3 and PPT 5, a calibration curve of differential pressure as a function of angle of

attack for each Mach number is required. These steady-state calibration curves were initially predicted using engineering methods, then refined with wind-tunnel data. The block diagram in figure 7 shows these calibration curves implemented as two-dimensional table lookups.

The sensor selection routine is used to determine out-of-range or “failed” FADS sensors. Because the flight control system is single-string, the INS angle of attack is assumed to be an unfailed but biased estimate of true angle of attack. The INS angle of attack is passed through a first-order lag filter corresponding to each FADS angle-of-attack pneumatic lag model derived from wind-tunnel data. (This model will be described in the Results and Discussion section.) These lagged INS angle-of-attack signals are then compared to the three corresponding FADS angle-of-attack signals. A FADS angle-of-attack signal is considered “failed” if this comparison exceeds a threshold for a fixed length of time. The threshold is a function of Mach number and is dependent on the amount of lag that can be tolerated by the system.

The final FADS angle of attack is the average of the “unfailed” signals. This final FADS angle of attack is then used to bias the INS angle of attack through a first-order filter as shown in figure 7. If all FADS sensors are declared failed, the bias will fade to 0 and the uncompensated INS angle of attack is used in the flight control laws.

Other significant airdata parameters sensed by the FADS system are derived from postflight data using nonlinear regression algorithms. Reference 1 details how these postflight airdata estimation algorithms are developed.

Results and Discussion

This section discusses the data obtained in the wind-tunnel test. Results are compared with both predicted static pressure and simulated pneumatic lag results.

Steady-State Pressure

The calibration curves used to derive angle of attack from the pressure data were initially developed using engineering analysis. Newtonian flow theory was used to obtain stagnation pressure. Oblique shock theory or Prandtl-Meyer expansion methods,¹⁰ depending on angle-of-attack and flow conditions on the wedge, were used to solve for surface pressures on the wedge itself. A

wind-tunnel test was then conducted to validate the initial pressure model of the FADS system.

Figures 8(a)–(d) show the comparison of the predicted pressure model and the wind-tunnel data as a function of angle of attack for Mach numbers of 3, 4, and 8. The wind-tunnel data are shown as open symbols and the predicted data are shown as solid symbols. Results for the other Mach numbers listed in table 3 are similar to the Mach 8 results.

Results from port 2 (fig. 8(a)) indicate that the predicted pressures compare very well with the wind-tunnel pressures. Results from port 4 (fig. 8(c)) indicate similar results; the exception is the Mach 8 case in which pressure for the high angles of attack was underpredicted. This slight underprediction may be caused by flow separation at the high Mach numbers.

The two rear ports (ports 3 and 5) show large differences, especially on the lower ramp port 5 (fig. 1). The results for port 3 (fig. 8(b)) indicate good agreement, except for the Mach 3 case in which a small slope change appears in the wind-tunnel results. The cause for this difference is unknown, but may be because of data acquisition errors. The results for port 5 (fig. 8(d)) indicate an overprediction of the pressures at the high angles of attack at Mach 3 and 4 and an underprediction at Mach 8. This difference is most likely caused by the presence of the boundary-layer trip strip located in front of port 5. The simple prediction models used for the wind-tunnel comparisons could not include a boundary-layer trip strip. The boundary-layer trip strip was installed on the model in a manner similar to that planned for the flight vehicle. Overall, the predicted pressures compared well with the wind-tunnel pressures for ports located forward of the boundary-layer trip strip. Additional corrections for boundary-layer trip strip effects could be developed for port 5 to reduce the errors even further.

Pressure data obtained from the wind-tunnel test were used as input to the angle-of-attack estimation routines previously described (fig. 7). True angle of attack and tunnel dynamic pressure were used as inputs instead of the INS parameters that will be used in the flight software. Figure 9 shows angle-of-attack error ($\alpha_{true} - \alpha_{FADS}$) across the angle-of-attack range for the same Mach numbers as shown in figure 8. Figure 9(a) shows the angle-of-attack error for the forward pair of ports, and figure 9(b) shows the angle-of-attack error for the aft pair of ports.

The angle-of-attack error shown for the forward ports generally is less than 0.2° at less than 6° angle of attack, and is less than 0.5° across the entire angle-of-attack envelope. These excellent results are consistent with the pressure results shown in figures 8(a) and 8(c). The results for the aft pair of ports show large angle-of-attack errors, especially at the high angles of attack. The trends in angle-of-attack error are consistent with the errors in predicted pressures shown in figures 8(b) and 8(d). The results show the viability of the real-time angle-of-attack estimation method.

Pneumatic Lag

Because the FADS system is pneumatically-based, pressure lags must be taken into account. For the current angle-of-attack estimation design, the pneumatic lag models are used in the sensor selection routine to determine out-of-range or “failed” FADS sensors. A pressure lag model was developed for each port (or pair of ports) in the system because tubes of different length were used for each sensor (figs. 1–2 and table 2). The pressure lag from each port to sensor was modeled as a first-order lag:¹³

$$\frac{P_{PPT}}{P_{port}} = \frac{k}{s + k}, \quad (2)$$

where k is a nonlinear function of the measurement geometry and the input pressure P_{port} . The lag constant, k , can be represented by the following form:

$$k = \frac{1}{\tau} = \frac{P_{port}}{\mu} \left[\frac{g \pi D^4}{128 L V_e} \right], \quad (3)$$

where D is the diameter of the tube, L is the tube length, and V_e is the effective volume. Equations (2) and (3) characterize the lag from a single port to an absolute pressure measurement.

Figure 10 shows wind-tunnel data from a Mach 6, dynamic, pitch-pause angle-of-attack sweep (-6° to 12°). As seen in the absolute pressure measurements (PPT 3 and PPT 5), the lag characteristics change significantly over the pressure range as predicted by equation (3). In contrast, the lag characteristic of the differential pressure transducer from a pair of ports (PPT 2) remains relatively constant across the pressure range. This empirical observation allows the differential pressure lags to be adequately characterized by equation (2) with a constant lag factor across the measurement

range. In other words, the lag model for a pair of ports to a differential pressure measurement is only a function of Mach and not a function of the input pressure, thus greatly simplifying the lag characterization.

An analog matching technique was used to estimate the lag constant for the differential pressure signals across the angle-of-attack measurement range. True angle of attack was converted to unlagged pressure by using the inverse angle-of-attack estimation algorithm shown in figure 7. The resulting pressure was then used as an input to a constant first-order lag model to obtain the simulated pressure at the PPT. The lag constant was varied in order to minimize the error between the lagged results and the actual differential pressure signal, and thus to obtain the best fit over the entire range.

Figure 11 shows a typical result for one of the pitch-pause angle-of-attack sweeps (at Mach 6). A time history of scaled true angle of attack is shown with the actual and simulated differential pressure for the forward pair of ports. Three sections of the time history are magnified to show the very good agreement between the simulated and actual signals, especially in the low-angle-of-attack range. These results show that the pneumatic lags can be characterized by a first-order lag, where the lag constant is only a function of Mach.

Figure 12 is a summary of the lag characterization for all three FADS angle-of-attack signals across the tested Mach number range. These lags are accounted for in the real-time algorithm as previously described in the Real-Time Angle-of-Attack Estimation Algorithm section.

Concluding Remarks

The design of a flush airdata sensing (FADS) system for a sharp-nosed, wedge-shaped vehicle has been described. Real-time angle-of-attack estimation from the FADS system can be used to bias an inertial navigation system angle of attack.

Wind-tunnel tests were conducted to validate the predicted static and dynamic characteristics of the FADS system. The predicted static pressures for a matrix of ports compared well with the wind-tunnel results. Calibration curves were developed to convert differential pressures to angle of attack. Using ports forward of the boundary-layer trip strip results in angle-of-attack errors less than 0.2° at less than 6° angle of attack, and less than 0.5° for the entire angle-of-attack range.

Based on dynamic wind-tunnel results, characterizing the lag from a pair of ports to a differential transducer as a constant first-order lag is possible. The pneumatic lag models are used to determine out-of-range or “failed” FADS sensors in the real-time angle-of-attack algorithm.

Wind-tunnel results for static and dynamic pressure data validate the prediction models and the FADS architecture. The wind-tunnel results show that the performance of a FADS system for a sharp-nosed, wedge-shaped vehicle can be designed to meet the requirements for accurate measurement of angle of attack for real-time control and for postflight analysis.

References

- ¹Whitmore, Stephen A. and Timothy R. Moes, *Measurement Uncertainty and Feasibility Study of a Flush Airdata System for a Hypersonic Flight Experiment*, NASA TM-4627, 1994.
- ²Enns, Dale F., Dan J. Bugajski, John Carter, and Bob Antoniewicz, “Multi-Application Controls: Robust Nonlinear Multivariable Aerospace Controls Applications,” *Fourth High Alpha Conference*, CP-10143, vol. 2, 1994.
- ³Cary, John P. and Earl R. Keener, *Flight Evaluation of the X-15 Ball-Nose Flow-Direction Sensor as an Air-Data System*, NASA TN-D-2923, 1965.
- ⁴Siemers, Paul M. III, Martin W. Henry, and James B. Eades, Jr., “Shuttle Entry Air Data System (SEADS)—Advanced Air Data System Results: Air Data Across the Entry Speed Range,” *Orbiter Experiments (OEX) Aerothermodynamics Symposium*, CP-3248, Part 1, Apr. 1995, pp. 49–78.
- ⁵Larson, Terry J., Stephen A. Whitmore, L. J. Ehernberger, J. Blair Johnson, and Paul M. Siemers III, *Qualitative Evaluation of a Flush Air Data System at Transonic Speeds and High Angles of Attack*, NASA TP-2716, 1987.
- ⁶Whitmore, Stephen A., Timothy R. Moes, and Terry J. Larson, *Preliminary Results From a Subsonic High Angle-of-Attack Flush Air Data Sensing (HI-FADS) System: Design, Calibration, and Flight Test Evaluation*, NASA TM-101713, 1990.
- ⁷Whitmore, Stephen A., Brent R. Cobleigh, and Edward A. Haering, *Design and Calibration of the X-33 Flush Airdata Sensing (FADS) System*, NASA TM-1998-206540, 1998.

⁸Anderson, John D., Jr., *Hypersonic and High Temperature Gas Dynamics*, McGraw-Hill Book Company, New York, 1989.

⁹Solid State Electronics Center, *Precision Pressure Transducer PPT and PPT-R: User's Manual Version 2.4*, Honeywell, Inc., 1996.

¹⁰Ames Research Staff, *Equations, Tables, and Charts for Compressible Flow*, Report 1135, 1953.

¹¹Boudreau, A. H., *Performance and Operational Characteristics of AEDC/VKF Tunnels A, B, and C*, AEDC-TR-80-48, July 1981.

¹²Avallone, Eugene A. and Theodore Baumeister III, eds., *Marks' Standard Handbook for Mechanical Engineers*, 10th ed., McGraw-Hill, Boston, Massachusetts, 1996.

¹³Lamb, J. P., Jr., *The Influence of Geometry Parameters Upon Lag Error in Airborne Pressure Measuring Systems*, WADC TR-57-351, July 1957.

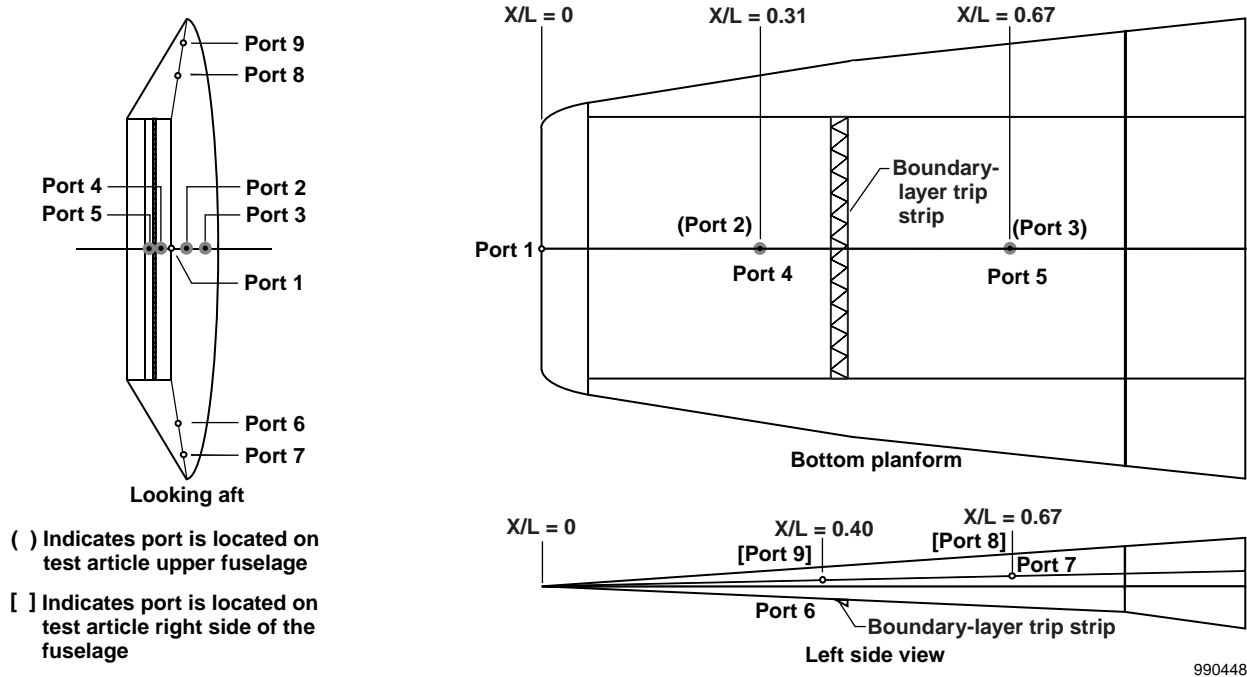


Figure 1. Test article pressure port locations.

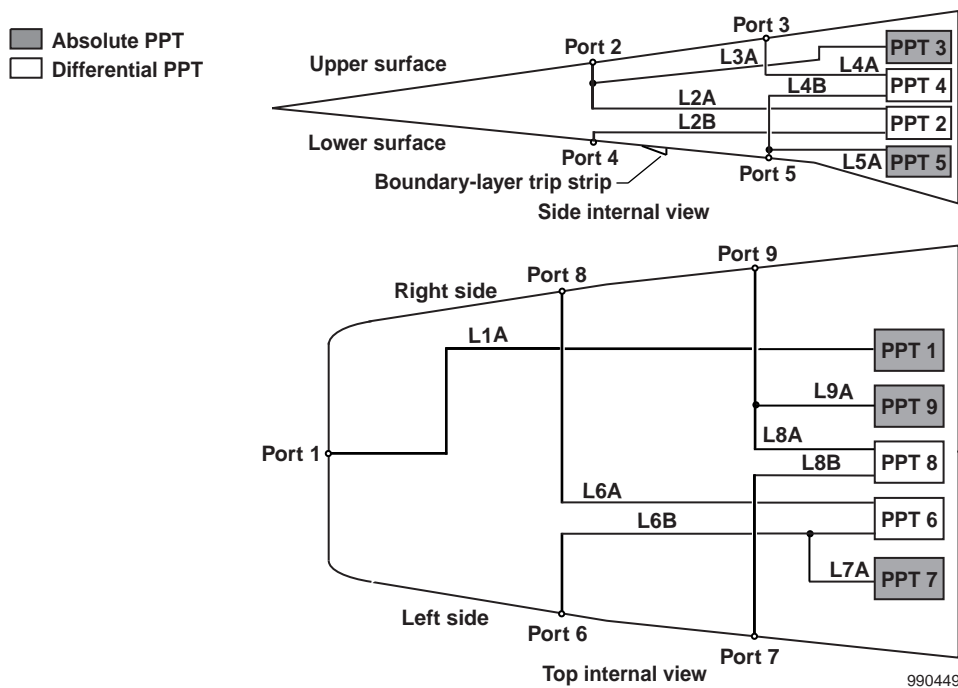


Figure 2. Wind-tunnel model pressure transducer connectivities.

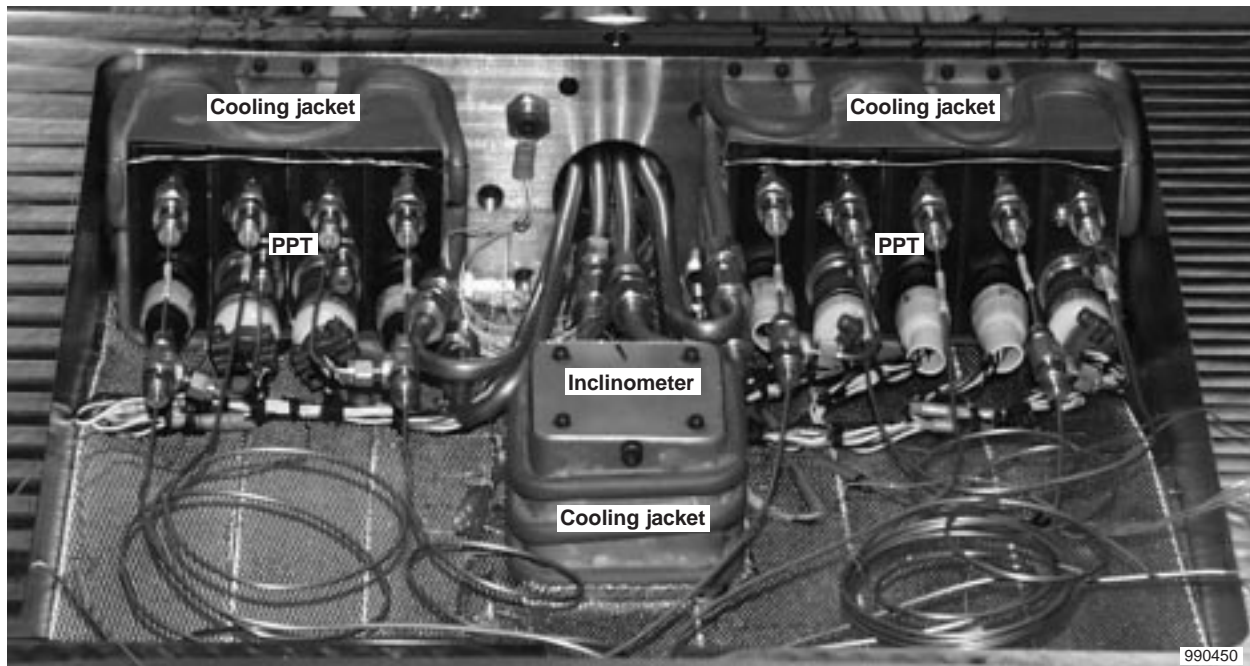


Figure 3. Internal layout of wind-tunnel model.

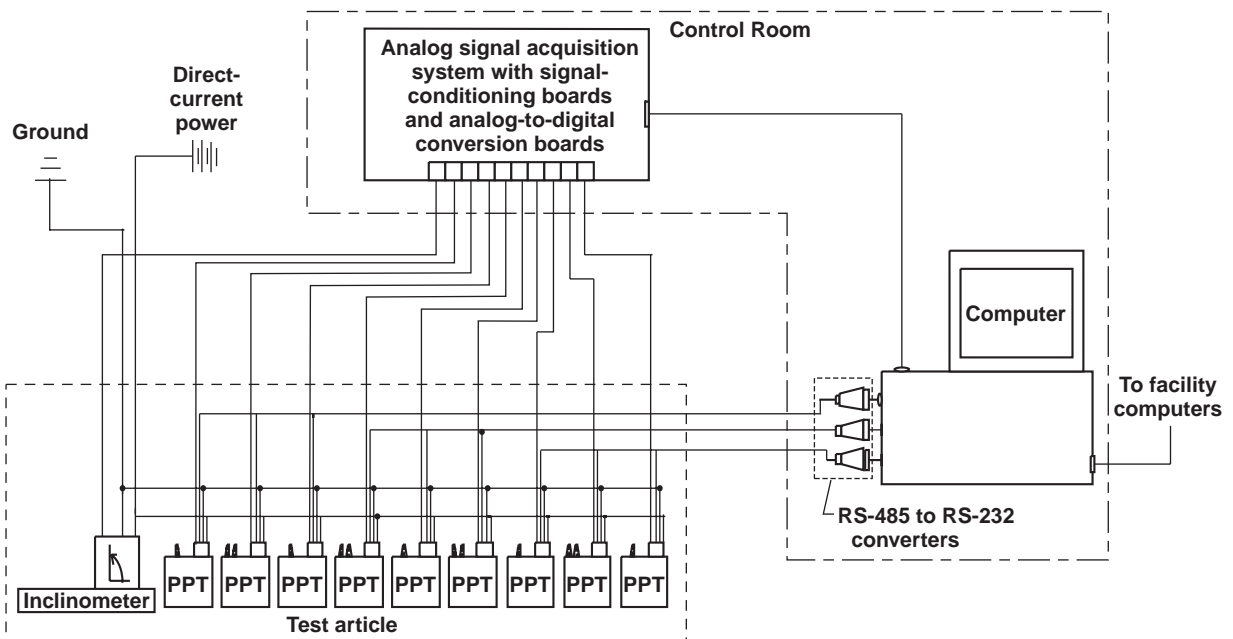
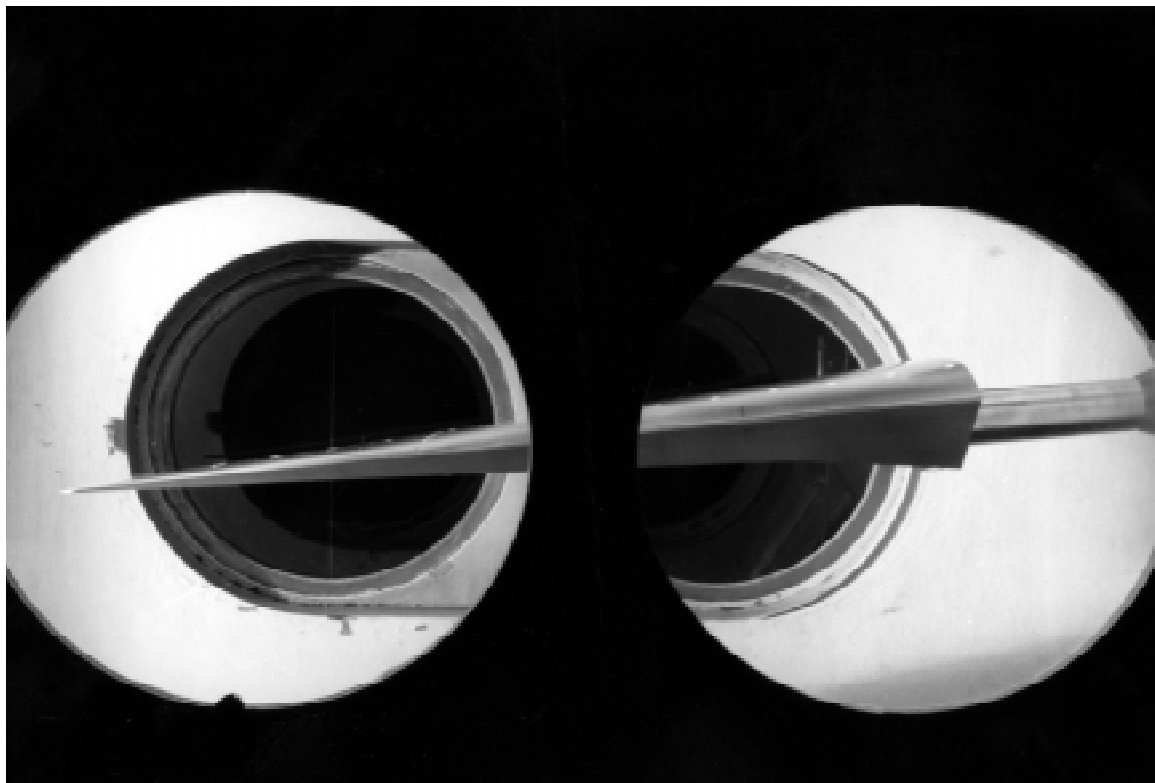


Figure 4. Wind-tunnel test setup.



Photograph courtesy of U. S. Air Force, AEDC, 98-104210.

Figure 5. Test article in Tunnel A test section.



Photograph courtesy of U. S. Air Force, AEDC, 98-106729.

Figure 6. Test article in Tunnel B test section.

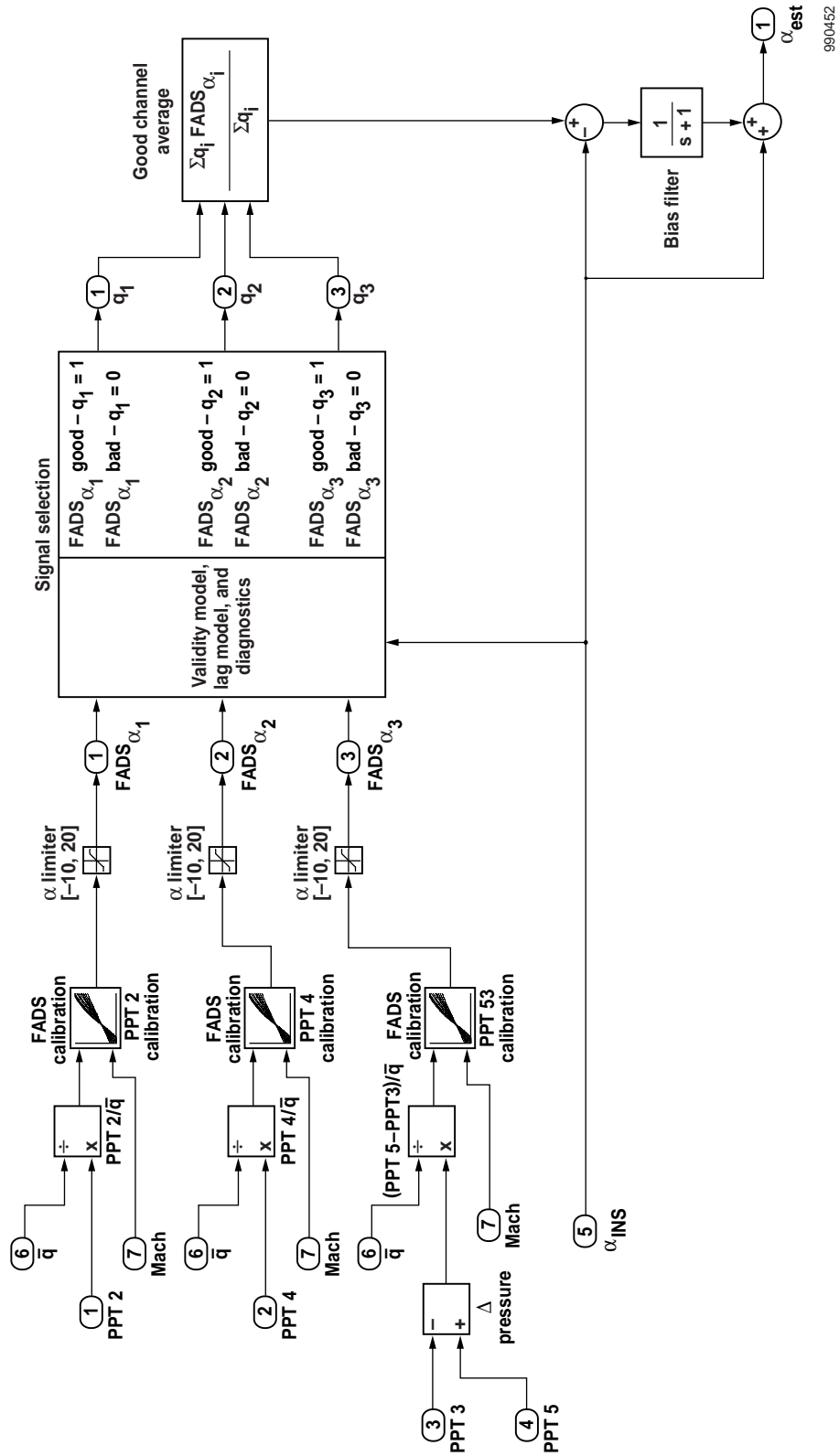
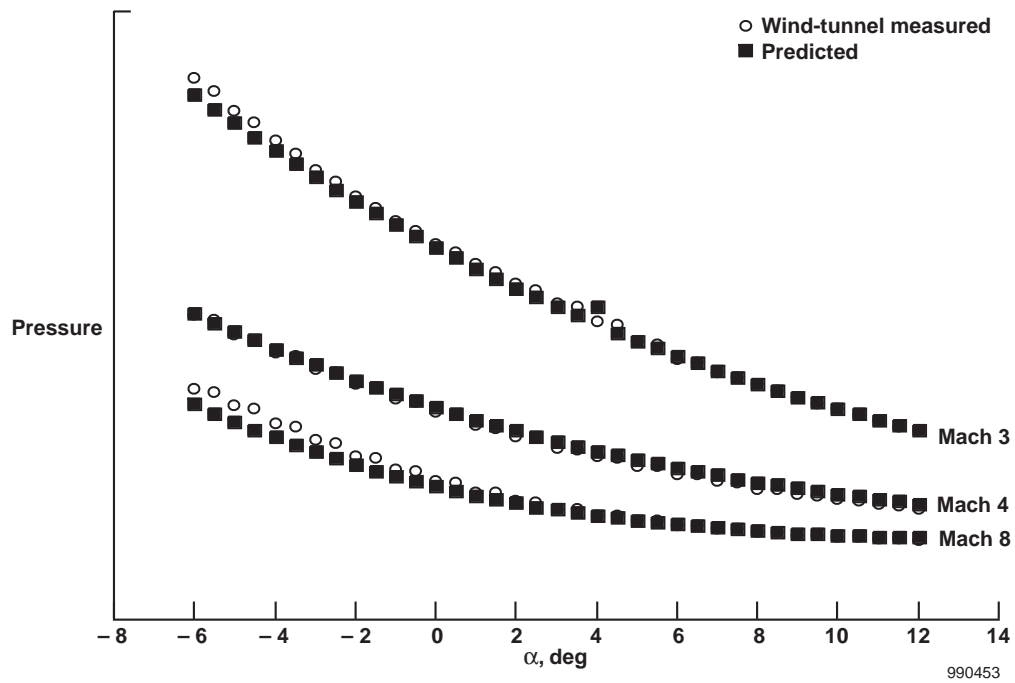
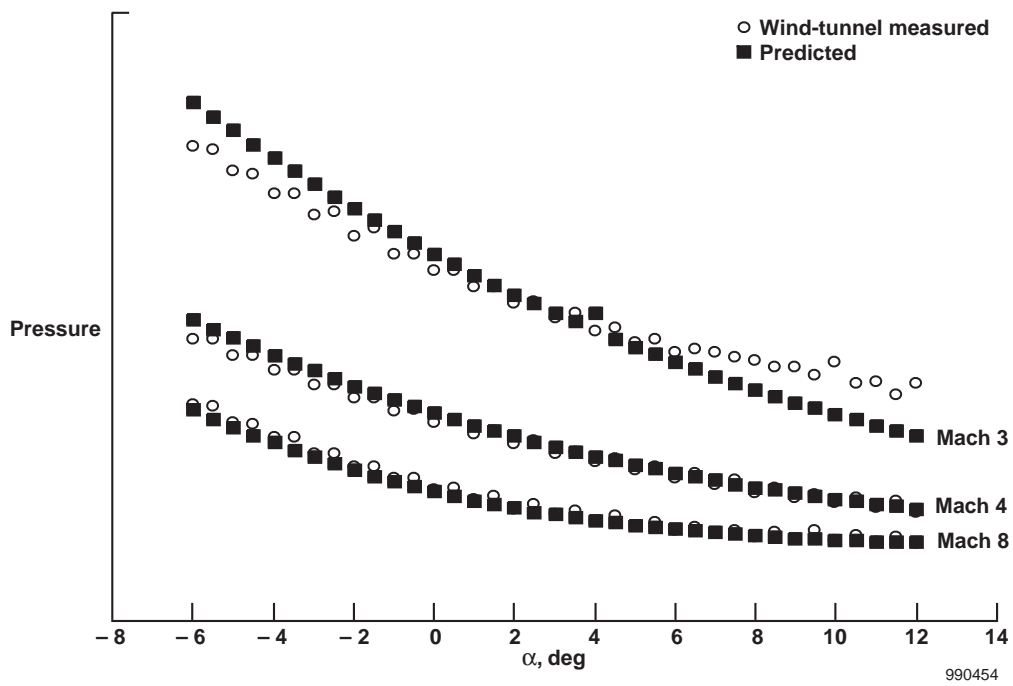


Figure 7. α_{FADS} and α_{INS} estimation and integration block diagram.

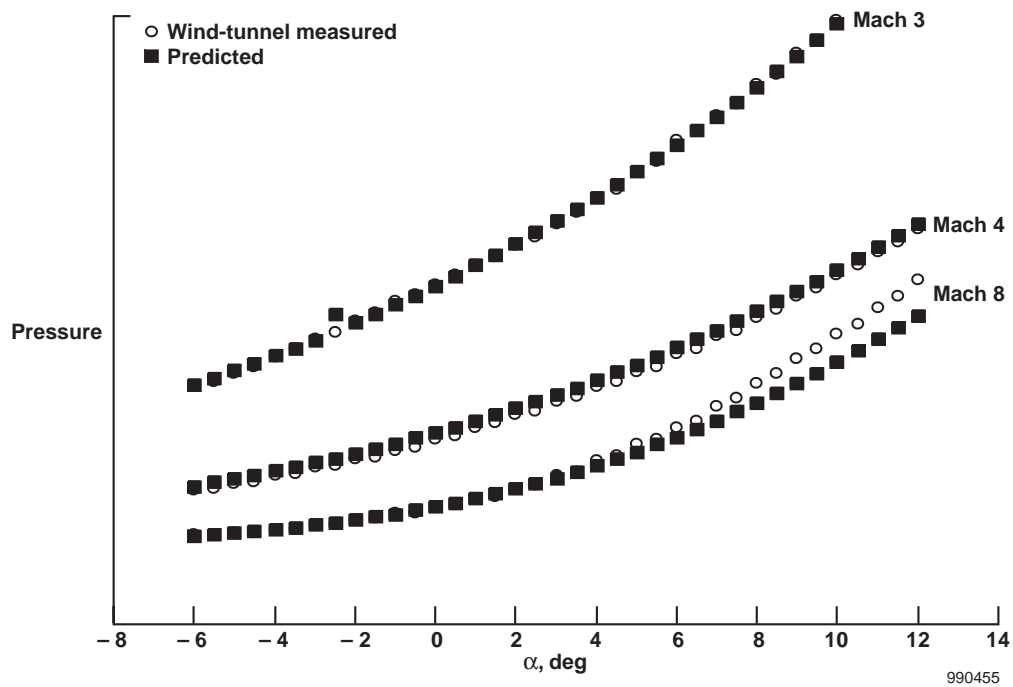


(a) Pressure as a function of angle of attack for port 2.

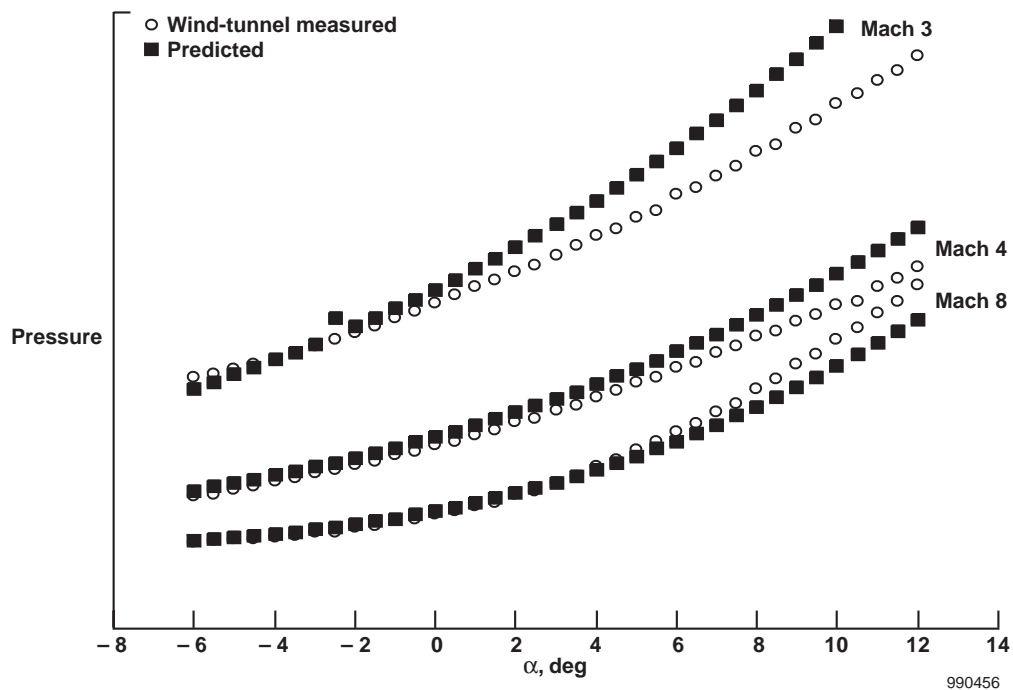


(b) Pressure as a function of angle of attack for port 3.

Figure 8. Comparison of empirical and wind-tunnel data for the α_{FADS} .

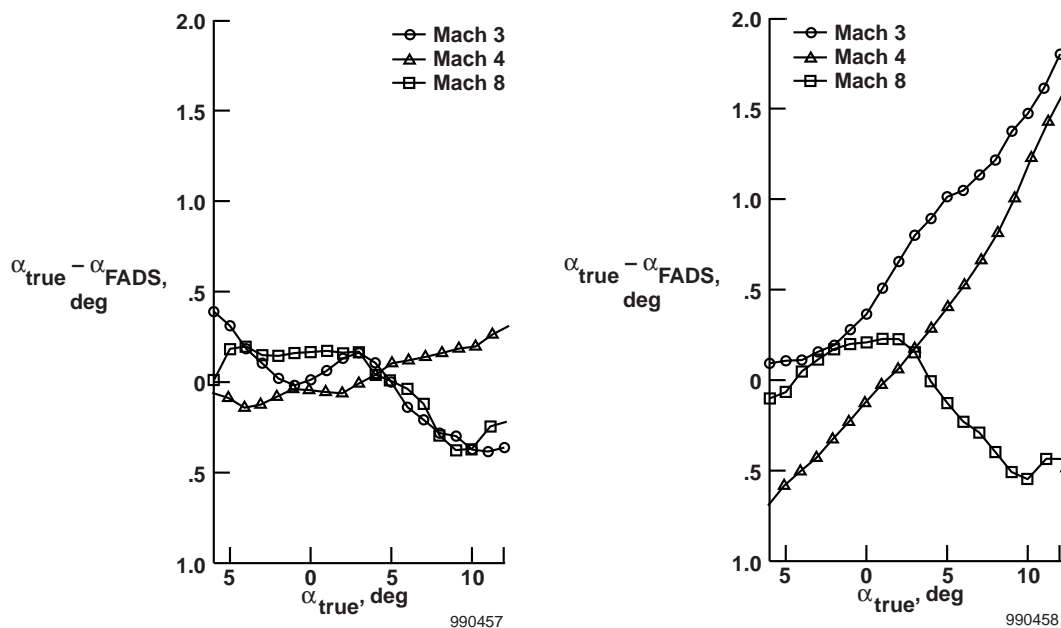


(c) Pressure as a function of angle of attack for port 4.



(d) Pressure as a function of angle of attack for port 5.

Figure 8. Concluded.



(a) Forward ports ($FADS_{\alpha_1}$).

(b) Aft ports ($FADS_{\alpha_2}$ and $FADS_{\alpha_3}$).

Figure 9. Angle-of-attack error ($\alpha_{true} - \alpha_{FADS}$) as a function of true angle of attack.

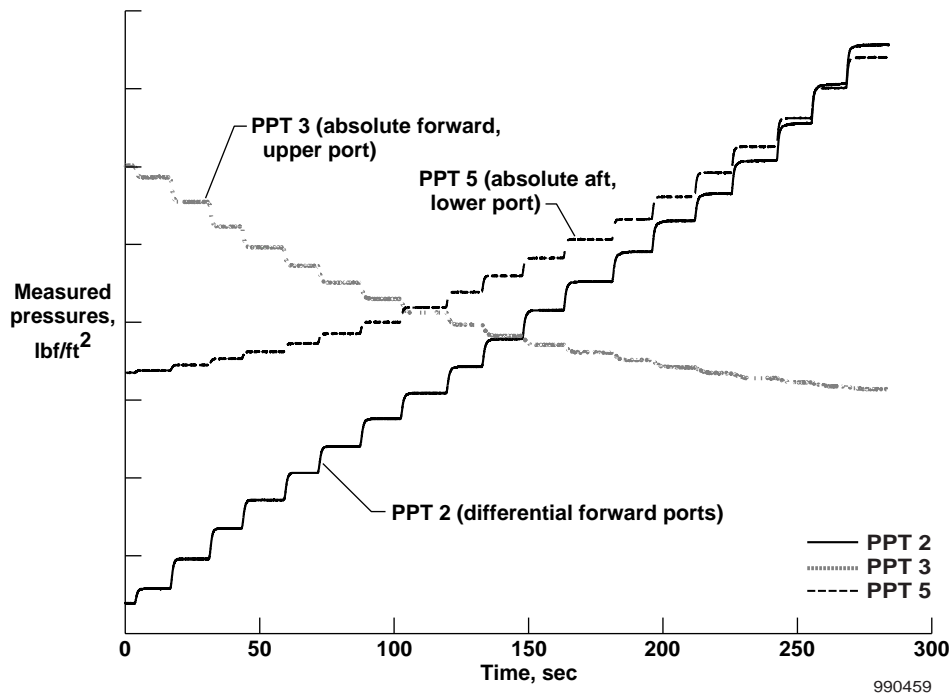


Figure 10. Typical wind-tunnel pitch-pause angle-of-attack sweep for Mach 6.

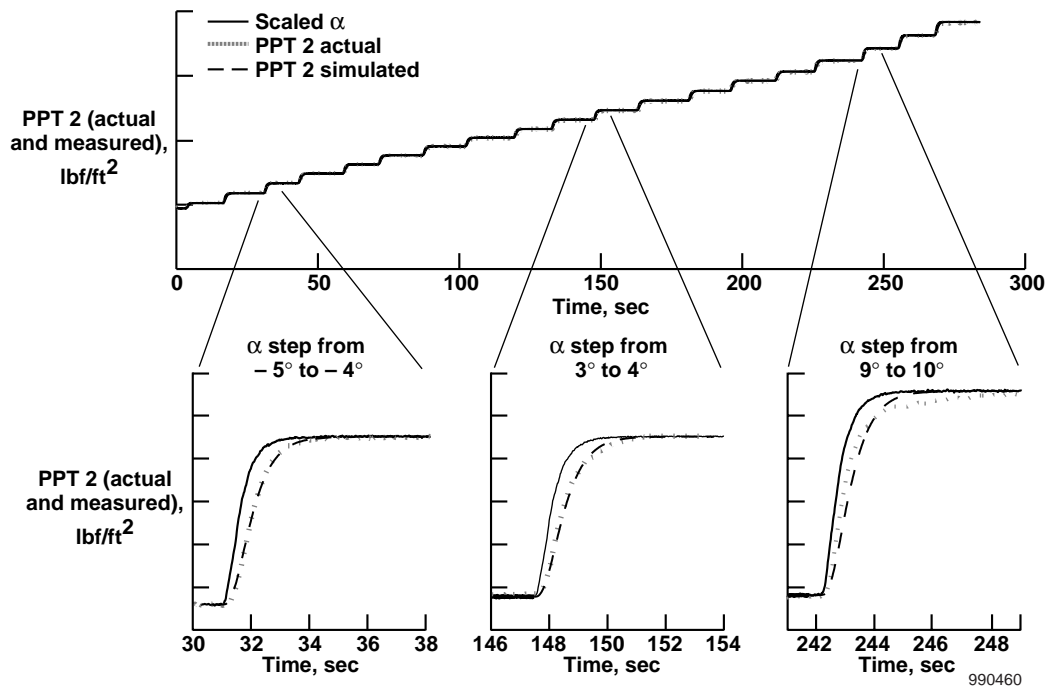


Figure 11. Simulated and actual pressure lag characteristics for Mach 6 pitch-pause angle-of-attack sweep.

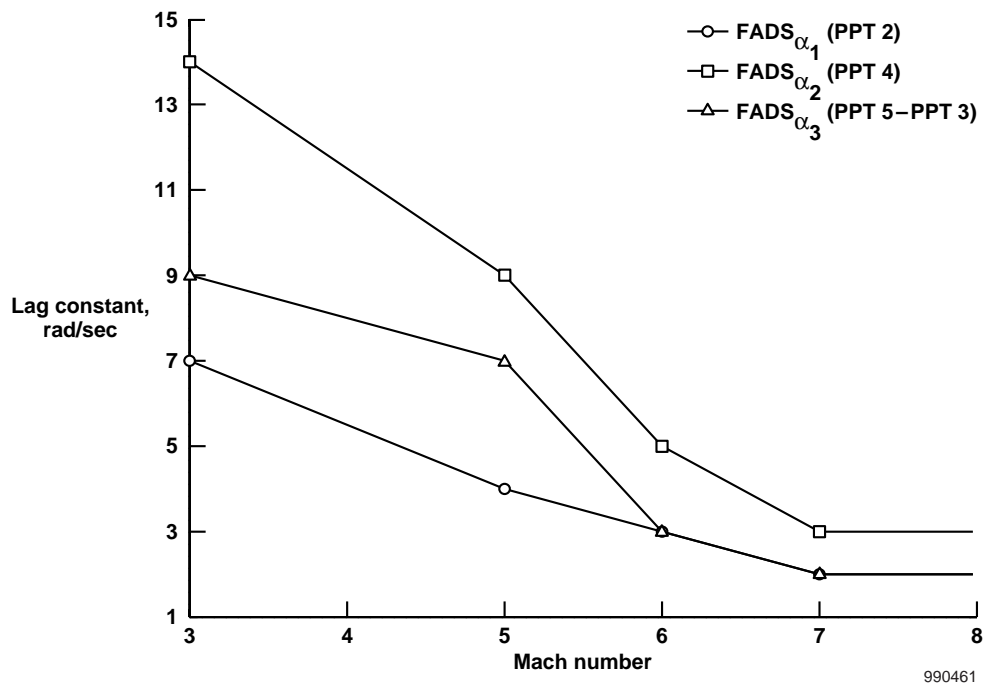


Figure 12. Summary of lag characteristics for all three angle-of-attack estimations as a function of Mach number.

REPORT DOCUMENTATION PAGE

Form Approved
OMB No. 0704-0188

Public reporting burden for this collection of information is estimated to average 1 hour per response, including the time for reviewing instructions, searching existing data sources, gathering and maintaining the data needed, and completing and reviewing the collection of information. Send comments regarding this burden estimate or any other aspect of this collection of information, including suggestions for reducing this burden, to Washington Headquarters Services, Directorate for Information Operations and Reports, 1215 Jefferson Davis Highway, Suite 1204, Arlington, VA 22202-4302, and to the Office of Management and Budget, Paperwork Reduction Project (0704-0188), Washington, DC 20503.

1. AGENCY USE ONLY (Leave blank)		2. REPORT DATE January 2000	3. REPORT TYPE AND DATES COVERED Conference Paper	
4. TITLE AND SUBTITLE Development of a Flush Airdata Sensing System on a Sharp-Nosed Vehicle for Flight at Mach 3 to 8			5. FUNDING NUMBERS WU 522-51-54-00-50-00-X43	
6. AUTHOR(S) Mark C. Davis, Joseph W. Pahle, John Terry White, Laurie A. Marshall, Michael J. Mashburn, and Rick Franks				
7. PERFORMING ORGANIZATION NAME(S) AND ADDRESS(ES) NASA Dryden Flight Research Center P.O. Box 273 Edwards, California 93523-0273			8. PERFORMING ORGANIZATION REPORT NUMBER H-2390	
9. SPONSORING/MONITORING AGENCY NAME(S) AND ADDRESS(ES) National Aeronautics and Space Administration Washington, DC 20546-0001			10. SPONSORING/MONITORING AGENCY REPORT NUMBER AIAA 2000-0504	
11. SUPPLEMENTARY NOTES Paper presented at 38th AIAA Aerospace Sciences Meeting and Exhibit, 10-13 January 2000, Reno, NV, AIAA 2000-0504. M. Davis, J. Pahle, J. White and L. Marshall of NASA Dryden Flight Research Center, Edwards, CA. M. Mashburn of Micro Craft, Inc., Tullahoma, TN. Rick Franks of Sverdrup Corp., Arnold AFB, TN.				
12a. DISTRIBUTION/AVAILABILITY STATEMENT Unclassified—Unlimited Subject Category 06 This report is available at http://www.dfrc.nasa.gov/DTRS/			12b. DISTRIBUTION CODE	
13. ABSTRACT (Maximum 200 words) NASA Dryden Flight Research Center has developed a flush airdata sensing (FADS) system on a sharp-nosed, wedge-shaped vehicle. This paper details the design and calibration of a real-time angle-of-attack estimation scheme developed to meet the onboard airdata measurement requirements for a research vehicle equipped with a supersonic-combustion ramjet engine. The FADS system has been designed to perform in flights at Mach 3–8 and at -6° – 12° angle of attack. The description of the FADS architecture includes port layout, pneumatic design, and hardware integration. Predictive models of static and dynamic performance are compared with wind-tunnel results across the Mach and angle-of-attack range. Results indicate that static angle-of-attack accuracy and pneumatic lag can be adequately characterized and incorporated into a real-time algorithm.				
14. SUBJECT TERMS Airdata calibration, FADS, Flush airdata sensing system, Hypersonics, Wedge forebody, Wind tunnel test			15. NUMBER OF PAGES 17	
			16. PRICE CODE	
17. SECURITY CLASSIFICATION OF REPORT Unclassified	18. SECURITY CLASSIFICATION OF THIS PAGE Unclassified	19. SECURITY CLASSIFICATION OF ABSTRACT Unclassified	20. LIMITATION OF ABSTRACT Unlimited	